New direction in nanotube science

M. Terrones[a*], A. Jorio[b], M. Endo[c], A. M. Rao[d], Y. A. Kim[c], T. Hayashi[c], H. Terrones[a], J.-C. Charlier[e], G. Dresselhaus[f], and M. S. Dresselhaus[g]

We review the latest advances in the production and state-of-the art characterization of B- and N-doped carbon nanotubes (CNTs) and nanofibers. We briefly discuss different approaches to producing these novel doped nano-systems. The use of high-resolution transmission electron microscopy (HRTEM), electron energy loss spectroscopy (EELS), scanning tunneling spectroscopy (STS), Raman spectroscopy, and allied techniques to characterize these doped systems is reviewed. The field emission properties as well as some applications to the fabrication of novel polymer composites, Li^+ batteries, and gas sensors are also discussed. It is clear that these materials possess outstanding properties when compared with pure CNTs, and it is foreseen that these systems will revolutionize some aspects of nanotube science and technology, thus opening a vast field of experimental and theoretical research.

[a*] Advanced Materials Department, IPICYT, Camino a la Presa San José 2055, Col. Lomas 4a. sección, San Luis Potosí 78216, SLP, México
E-mail: mterrones@ipicyt.edu.mx

[b] Universidade Federal de Minas Gerais – UFMG, Depto de Física – Icex, C. Postal: 702 – CEP: 30123970, Belo Horizonte MG, Brasil

[c] Faculty of Engineering, Shinshu University 4-17-1 Wakasato, Nagano-shi 380-8553 Japan

[d] Department of Physics and Astronomy, Clemson University, South Carolina 29634, USA

[e] Université Catholique de Louvain, PCPM & CERMIN, B-1348 Louvain-la-Neuve, Belgium

[f] Francis Bitter Magnet Laboratory, Massachusetts Institute of Technology, Cambridge, MA 02139, USA

[g] Department of Physics, and Department of Electrical Engineering and Computer Science, Massachusetts Institute of Technology, Cambridge, MA 02139, USA

Carbon is a versatile element and it has been demonstrated that it can form various allotropes, including graphite, diamond, and fullerene-like structures[1-3]. In particular, graphite is a semimetal and, when a single sheet of the carbon honeycomb is rolled, it is possible to generate seamless carbon cylinders (termed nanotubes), which can be either metallic or semiconducting, depending on their diameter and chirality[1-3] (see Textbox 1).

In layered sp^2 carbon systems, it is possible to tailor the electronic, vibrational, chemical, and mechanical properties by replacing some of the carbon (C) atoms with either boron (B) or nitrogen (N). In particular, B and N contain one electron less and one electron more as compared with C, respectively. For example, if B replaces some C atoms in the graphene sheet, the electronic structure contains electronic *holes*, responsible of generating a *p*-type conductor, whereas when N atoms substitute for C atoms, the formation of an *n*-type material arises (see Textbox 2).

In the past, various groups have doped graphite with B atoms in order to enhance its crystallinity and graphitization (e.g. reduction of the interlayer spacing and slight increase in the in-plane distances)[4,5]. Almost 40 years ago, Lowell[4] reported that only 2.35 at% of B can be incorporated in the graphite lattice in order to reduce the interlayer spacing (d_{002}) in the doped layers. This incorporation occurs via solid solution processes and involves high temperatures (2200°C)[4]. Oya and coworkers[6] have also demonstrated that B concentrations in excess of 5 at% within graphitic systems result in the formation of B_4C as a byproduct. For lower temperature processes (e.g. 600-900°C) involving B atoms in

ISSN:1369 7021 © Elsevier Ltd 2004

Textbox 1

Nanotube structure can be mathematically defined in terms of a chiral vector $\boldsymbol{C_h}$ ($\boldsymbol{C_h} = n\boldsymbol{a_1} + m\boldsymbol{a_2}$), which can determine the tube diameter d_t. This vector determines the rolling direction of a graphene sheet, in which a lattice point (n,m) is superimposed with an origin defined as (0,0). Thus, the diameter can be expressed as,

$$d_t = a\sqrt{(m^2 + nm + n^2)}/\pi$$

where a = 1.42 x $\sqrt{3}$ Å and corresponds to the lattice constant in the graphite sheet. Note that the C-C distance is 1.42 Å.

In order to determine the armchair and zigzag structures in terms of (n,m) and the chiral angle θ, it is necessary to have the following conditions:

$\theta = 0$, $(n,m) = (p,0)$, where p is an integer (zigzag)

$\theta = \pm 30°$, $(n,m) = (2p,-p)$ or (p,p) (armchair)

The chiral angle θ (angle between $\boldsymbol{C_h}$ and the zigzag direction) is defined as: $\theta = \arctan[-\sqrt{3}m/(2n + m)]$.

CNTs can be either metallic or semiconducting depending on the choice of (n,m). The metallic conductivity condition for these tubular structures can be written:

$(2n + m)/3 =$ integer

These unique electronic properties arise from quantum confinement of electrons normal to the nanotube axis. In the radial direction, electrons are confined by the monolayer thickness of the graphene sheet.

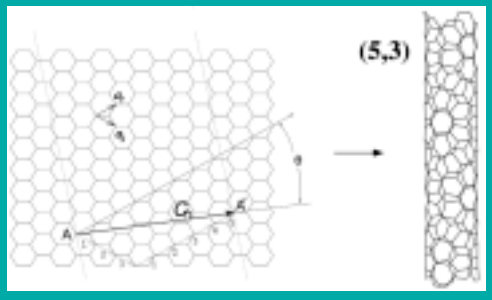

layered carbon systems, higher concentrations of B could be incorporated. However, the structure becomes more disordered, possibly by the creation of interstitial B atoms, which restrict ordering of the hexagonal layers[5]. In general, it can be concluded that B aids the graphitization of laminar carbons if it replaces C atoms in the hexagonal lattice at defined low concentrations (e.g. <1%). If the B content increases, interstitials start to disrupt the layered structure.

Early work on the mechanical properties of B-doped polyacrylonitrile (PAN) fibers revealed an enhancement of the elastic modulus, maintaining the tensile strength of the doped fiber[7]. In addition, some B-doped carbon fiber composites (0.67 at% B) have enhanced oxidation resistance, three times larger than undoped carbon composites[5].

These bulk graphites doped with B behave like *p*-type conductors. Endo and coworkers have demonstrated using scanning tunneling microscopy (STM)[8] that B-doped, highly oriented pyrolytic graphite (HOPG) exhibits areas of extreme intensity (1 nm in diameter), where B atoms have substituted for C atoms in the hexagonal lattice (Fig. 1). Each bright area consists of B atoms with the highest electron density located in the center of six surrounding medium intensity sites that correspond to C atoms. The presence of these high intensity spots is caused by the presence B atoms, which induce intense localized states in the valence band close to the Fermi level, E_f, thus enhancing the tunneling current. These structural results suggest that B doping can contribute to

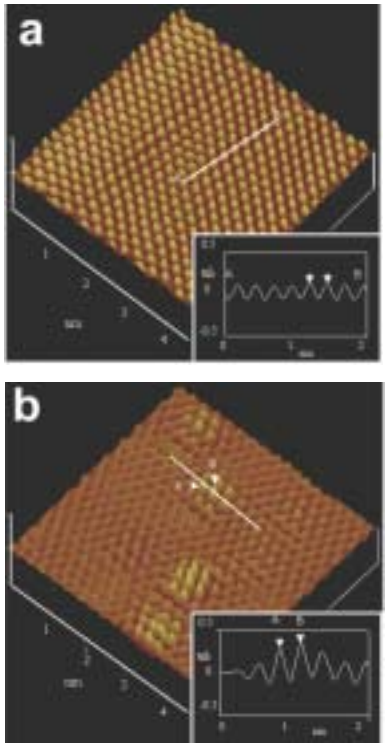

Fig. 1 STM images, using a three-dimensional surface plot and section analysis, corresponding to the line indicated (see insets) of the (a) HOPG and (b) B-doped HOPG graphene surfaces. Note the high intensity areas arising from the B atoms, responsible for creating intense localized electronic states close to the Fermi level in the valence band. In particular, the B site in the graphene network appears as the brightest area in the image including the six adjacent C atoms, which have relatively higher intensity than normal C atoms in the image (see peaks A and B in Fig. 1b inset). (Reprinted with permission from[8]. © 2001 American Institute of Physics.)

control of the properties of the hexagonal carbon network in order to modify its properties relative to those of ideal graphite. From an applications point of view, B-doped HOPG and fibers are now being used in the fabrication of composite anodes for Li^+ batteries with increased capacity (15-20% higher than conventional *undoped* anodes)[9].

For N-doped bulk graphitic systems, it was shown more than 30 years ago that N atoms tend to introduce disorder in the graphene planes, even at relatively low levels (e.g. <6.5 wt%)[10-12]. Thermal annealing above 2500°C displaces most N atoms, but traces of N (<0.5%) are still present in the carbon structure[10]. More recently, Belz *et al.*[13] reported the synthesis of N-doped carbons produced at high temperatures (>2500°C). The authors were able to introduce N within sp^2-like carbons ranging from 0.7-4.5 at%. X-ray photoelectron spectroscopy (XPS) studies reveal that N bonds to C in a nitrile- and pyridine-like fashion. This particular N-doped carbon material shows enhanced oxidation resistance, when compared with its pure carbon counterpart and the N content does not vary upon heating in vacuum at 500°C. From an electronic point of view, one expects to observe an excess of donors in the N-rich areas, which should be more reactive than crystalline graphite. Unfortunately, the literature on this issue is scarce.

B- and N-doped carbon materials

If a single-walled carbon nanotube (SWNT) is doped with either B or N, the electronic properties will be different from bulk doped-graphite. The quantum confinement and curvature of the cylinders will result in novel electronic, mechanical, and chemical properties, which are also different from their undoped counterparts. In particular, substitutional doping of B and N within graphene nano-cylinders will introduce strongly localized electronic features in the valence or conduction bands, respectively (see Textbox 2), and will enhance the number of electronic states at the Fermi level depending on the location and concentration of dopants.

Little work has been carried out in doping SWNTs with either B or N, but we believe that these systems should exhibit unusual quantum effects, and it should be possible to tailor the band gaps of semiconducting SWNTs when doping at very low concentration levels. Therefore, experimental and theoretical work is needed in order to exploit the possibility of doping quantum carbon wires. This review is targeted to motivate a new field in nanotube science, thus breaking new ground in the physics and chemistry of one-dimensional carbon systems. There are numerous challenges that we must overcome before producing N- and B-doped SWNTs in a controlled way, but it is clear that these materials will be

Textbox 2

Calculated density of states (DOS) using tight-binding parameters fitted with *ab initio* calculations[62] for: (a) an infinite graphene sheet doped with B (0.5 at%), in which the low concentration of B (solid line), playing the role of electronic acceptors, starts to increase the number of electronic states in the valence band, thus provoking a slight increase and shift of electronic states close to E_f; (b) an infinite graphene sheet doped with N (0.5 at%), in which the low concentration of N, playing the role of electronic donors, increases the number of electronic states in the conduction band (solid line), thus provoking a slight shift of electronic states close to E_f; (c) an armchair (10,10) B-doped (0.2 at%, solid line) CNT exhibiting a clear peak in the valence band (arrow); and (d) an armchair (10,10) N-doped (0.2 at%, solid line) CNT in which a sharp localized peak arises in the conduction band (arrow). Solid lines correspond to the doped materials, whereas dotted lines relate to pure C structures (undoped). Note that for all cases the presence of B introduces states in the valence band (holes), whereas N injects electrons in the conduction band (donors). Because of quantum confinement within CNTs, electrons only propagate along the nanotube axis, so their wave vectors point in this direction. The resulting number of one-dimensional conduction and valence bands effectively depends on the standing waves set up around the circumference of the nanotube. The spikes shown in the DOS of the tubules are called 'van Hove' singularities and are the typical signature of one-dimensional quantum conduction, which is not present in an infinite graphite crystal (calculations performed by S. Latil).

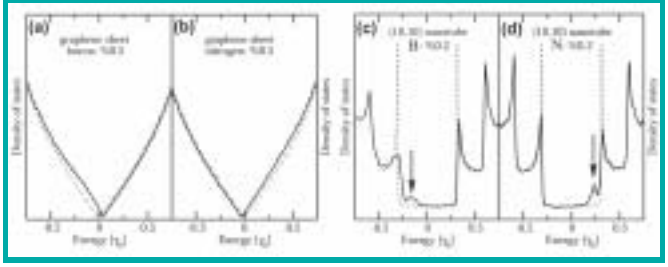

important in the fabrication of nanotube composites, electronic devices, sensors, nanobots, etc.

Besides graphite and SWNTs, it is also possible to dope double-walled (DWNTs) and multi-walled nanotubes (MWNTs) with B and/or N. In these systems, the electronic and mechanical properties change and new electronic, mechanical, and vibrational effects could be observed.

From the theoretical point of view, Hernández and coworkers have described the mechanical properties of CN_x and CB_x nanotubes[14,15], demonstrating that high concentrations of B and/or N within SWNTs lower the Young's modulus. Nevertheless, the Young's modulus values still remain on the order of 0.5-0.8 TPa. This phenomenon has been experimentally confirmed in pristine and N-doped MWNTs[16,17]. Unfortunately, the experimental values are quite different from the theoretical ones. For example, the Young's modulus for pristine and N-doped MWNTs are 0.8-1 TPa and ~30 GPa, respectively. We believe that the low values observed for N-doped nanotubes are the result of the relatively high N concentration (e.g. 2-5%) within the tubes, which introduces defects and lowers the mechanical strength. If the N concentration is <0.5%, it is expected that the mechanical properties will not be substantially altered.

B has one electron less than C, and when it substitutes for C atoms within a SWNT (three-coordinated B) sharp localized states below the Fermi level (valence band) appear (Textbox 2). These states are caused by the presence of holes in the structure, and the tube could be considered as a *p*-type nano-conductor. From the chemical standpoint, this structure would be more likely to react with donor-type molecules.

For N-doped SWNTs, two types of C-N bonds could occur in CNTs. The first is a substitutional N (N coordinated to three C atoms in a sp^2-like fashion), which induces sharp localized states above the Fermi level because of additional electrons, which are injected into the structure. These types of tubes exhibit *n*-type conduction, and are more likely to react strongly with acceptor molecules. The second type is a pyridine-type N (two coordinated N), which can be incorporated into the SWNT, provided that a C atom is removed from the framework. This type of defect induces localized states below and above the Fermi level. Therefore, substitutional N doping in SWNTs should result in *n*-type conducting behavior, whereas pyridine-type N may produce either a *p*- or *n*-type conductor, depending on the doping level, the number of N atoms, and the number of removed C atoms within the hexagonal sheet.

In order to observe genuine quantum effects in doped CNTs, dopants must be present within SWNTs of narrow diameter (<1-2 nm). In addition, we should point out that a low concentration of either B or N should not alter the mechanical properties and may enhance electron conduction if the number of foreign atoms is less than <0.5%.

Synthesis of doped nanotube materials

It is possible to synthesize either B- or N-doped CNTs using conditions far from equilibrium, similar to those used for producing pure CNTs. In the following paragraphs, these modified techniques are briefly summarized.

Arc method B-doped MWNTs can be produced in this way by arcing either BN/graphite or B/graphite electrodes in an inert atmosphere (e.g. He, N_2). In this case, large quantities of crystalline and *long* CNTs (≤100 μm) are obtained (Fig. 2a). In some cases, ill-formed caps containing B occasionally open or exhibit negative curvature regions (Fig. 2b)[18-20]. Using this technique, it has been difficult to produce B-doped SWNTs because B may frustrate the growth of the tubules under extreme conditions. Arc experiments using pure graphite electrodes in an NH_3 atmosphere indicate that it is also difficult to produce N-doped SWNTs and MWNTs, possibly because N_2 molecules are easily created and do not react with carbon[21]. Recently, Glerup *et al.*[22] demonstrated that it is possible to grow N-doped SWNTs by arcing composite anodes containing graphite, melamine, Ni, and Y. The authors demonstrate using EELS that the tubes exhibit a low

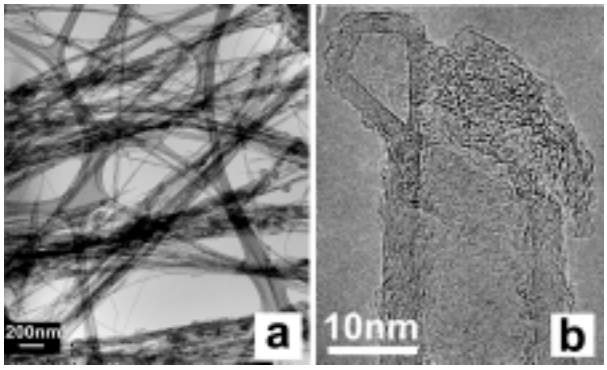

Fig. 2 (a) Low magnification TEM image of B-doped MWNTs produced by arc discharge (BN-graphite electrodes in a He atmosphere at 500 torr). Note that the tubes are long (>20 μm) and the number of polyhedral particles is significantly reduced; (b) HRTEM image of a B-doped MWNT exhibiting an ill-formed nanotube cap in which one segment of the tube is closed, adopting a diamond-like shape, while the other open end exhibits amorphous material around the tip containing B (revealed by EELS but not shown here).

concentration of N, <1%, and are sometimes corrugated because of their presence. The authors claim that EELS is able to detect low concentrations of dopants (e.g. 0.1%). This is mainly because the spectrometer used is very sensitive and unique. Therefore, further arc experiments and characterization should be conducted.

Laser ablation In 1997, Zhang *et al.*[23] reported that sandwich-like C-BN nanotubes could be produced by laser vaporization of graphite-BN targets. The authors reported evidence for the existence of BC_7N layers within the MWNTs and sometimes areas of segregated B and C were formed. Gai *et al.*[24] have recently demonstrated that it is possible to generate B-doped SWNTs using laser vaporization of B-graphite-Co-Ni targets. In particular, the authors carried out laser ablation experiments inside a silica tube, which was placed inside a furnace operating at 1100°C under an Ar atmosphere at ~500 torr. Subsequently, a laser beam (1064 nm, 10 Hz) was used to ablate a target[24] composed of a carbon paste mixed with Co:Ni catalyst (0.5:0.5 at%) and elemental B. The authors characterized the samples using HRTEM and EELS, and found SWNTs in the products when the B content in the target material was <3 at%. For higher B concentrations in the graphite target (e.g. >3.5 at%), most of the produced material consists of graphite and metal encapsulated particles; low quantities of SWNTs were obtained under these conditions. Therefore, these results are somewhat consistent with the previous work of Lowell[4] on graphite systems, in which it was difficult to incorporate a large concentration of B in the hexagonal framework. More experiments should now be conducted with N precursors using the laser technique, but it is likely that a large N content will result in the inhibition of SWNT growth. More energetic lasers (e.g. CO_2 or femtosecond lasers) should also be tested in order to generate N- or B-doped SWNTs.

Chemical vapor deposition (CVD) The thermal decomposition of hydrocarbons containing N over metal particles such as Fe, Co, and Ni results in the formation of N-doped MWNTs or CN_x nanotubes. It has been shown that only small concentrations of N (<15%)[25] can be introduced into MWNTs. The first report of the formation of aligned arrays of N-doped MWNTs[26] (<1-2%) involved the pyrolysis of aminodichlorotriazine over laser-etched Co thin films at 1050°C. In particular, the use of melamine (triaminotriazine) as a CN precursor results in an increased N content (<7%) within 'corrugated' carbon tubular structures. Aligned $C_{13}N_x$ ($x < 1$) nanotubes/nanofibers (<100 nm outer diameter, OD; <60 μm in length) are obtained in high yields by pyrolyzing melamine over laser-etched Fe substrates[27]. The results demonstrate that it is extremely difficult to generate crystalline and highly ordered structures containing large concentrations of N within the hexagonal carbon network. CN_x nanotubes with low N concentrations have been subsequently generated via pyrolysis of pyridine and methylpyrimidine[28]. Unfortunately, these CN_x nanotubes are easily oxidized (e.g. combustion sets in at ~450°C in air, whereas pure CNTs do not burn in air below ~700 °C)[28]. The degree of perfection within graphene sheets is highly dependent upon the N concentration (i.e. the lower the N content, the more 'graphitic' and straighter the nanotubes become).

However, it should be possible to generate SWNTs using this method if catalytic mixtures are used in conjunction with either CO or CH_4 and NH_3. For pure C, Dai *et al.*[29] have reported the generation of SWNTs using Mo particles in conjunction with CO (CO disproportionation) at 1200°C. Cheng *et al.*[30] have demonstrated that it is possible to obtain many SWNT ropes using experiments similar to those carried out by Endo in the 1970s[31]. In this case, the authors used thiophene as a sulfur source in addition to ferrocene and benzene. Therefore, N-doped SWNTs produced using CVD are plausible if low concentrations of NH_3 or an organic solvent containing N, such as pyridine, are used in conjunction with Fe, Co, Ni, MgO, Mo, S, etc. In this context, Keskar *et al.*[32] prepared isolated N-doped SWNTs from thermal decomposition of a xylene-acetonitrile mixture over nano-sized Fe catalyst particles. The N dopant concentration is controlled by the amount of acetonitrile in the mixture[32]. Unfortunately, not much work on doping SWNTs using this technique has been carried out.

It is expected that using B-containing organic precursors (e.g. boranes, boric acid, etc.) in conjunction with hydrocarbons and metal catalysts (e.g. Fe, Co, Ni) should produce MWNTs doped with B. However, there is still an enormous amount of work to be done in this area in order to control the B or N content, as well as the nanotube structure.

B and N substitution reactions: B- and N-doped SWNTs can also be produced using partial substitution in the presence of B_2O_3 vapor and N_2 at 1500-1700 K (Fig. 3)[33]. In these experiments, B-doped tubes exhibit a B/C ratio of <0.1. Lower amounts of N (N/C <0.01) can also be incorporated within

the hexagonal framework[33]. In contrast to B-doped MWNTs, SWNTs do not exhibit preferred chiralities, possibly because the dopants only substitute individual C atoms within the framework, thus preserving the tubule chirality. It is noteworthy that both B- or N-doped SWNTs show corrugation, attributable to defects on the C surface (Fig. 3).

Recently, Borowiak-Palen and coworkers[34] have reported the production of B-doped SWNTs with higher concentrations of B, in which 15% of the C atoms are replaced by B. These experiments[34] were conducted by heating B_2O_3 in the presence of pure C SWNTs and NH_3 at 1150°C. Thus, further studies on these samples should be carried out because the reported amount of B is too high compared with the solubility of B in graphite and MWNTs (<2 wt% B).

Plasma-assisted CVD: The microwave plasma-enhanced chemical vapor deposition technique (PECVD) has been used to synthesize large areas of aligned N-doped MWNTs[35-37]. These experiments involve catalytic particles of Fe and/or Ni dispersed on silica substrates. During growth at 500°C, acetylene or CH_4 and N_2 or NH_3 were used as the source gases. At relatively low to moderate CH_4 concentrations, the CNTs show a bamboo-type structure. This method grows well-aligned and separated individual MWNTs. To produce B- or BN-doped MWNTs by PECVD, other gases such as B_2H_6 in conjunction with H_2 and CH_4 could be used as the reacting gas[38]. However, these methods have not yet been exploited to produce SWNTs doped with either B or N. Thus, further and more detailed experiments should be carried out in the future using this powerful technique.

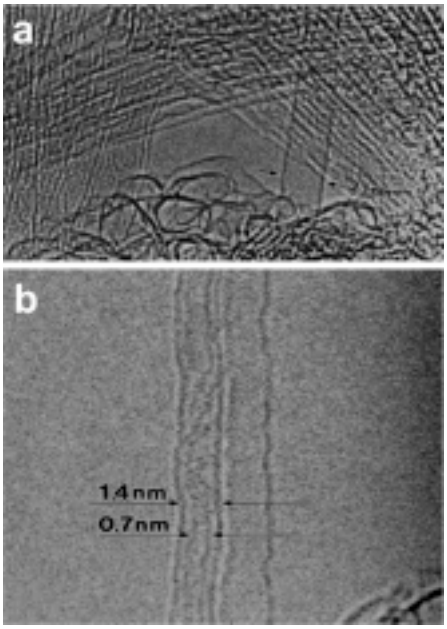

Fig. 3 (a) HRTEM image of an N-doped SWNT bundle synthesized at 1533 K over 240 minutes by reacting N_2, B_2O_3 with SWNT bundles of 1.4 nm diameter. Note the isolated SWNT exhibiting a diameter of 2.1 nm. (b) HRTEM image of a two-tube, B-doped bundle synthesized at 1503 K over 240 minutes by reacting N_2, B_2O_3 with SWNT bundles. The left-hand tube exhibits a SWNT with an inner shell (d = 0.7 nm) inside the outer shell (d = 1.4 nm). (Courtesy of D. Golberg).

Structure and characterization of doped CNTs

The most common techniques to visualize the structure and to characterize the morphology of MWNTs and SWNTs are: (a) HRTEM; (b) scanning electron microscopy (SEM); and (c) STM. In order to determine the overall crystalline structure of nanotubes, X-ray powder diffraction (XRD) is a powerful route. Electron diffraction (ED) has also proven useful in determining the chirality of tubes (the orientation of the hexagonal rings along the tube axis; zigzag, armchair, or chiral). An alternative route to determine the chirality of individual SWNTs is Raman spectroscopy, in which each SWNT has a characteristic radial breathing mode (RBM) associated with a particular diameter and, depending on the Raman laser line, it is possible to obtain resonance for particular tubules with specific electronic transitions. Because of the special relation between the geometric and electronic structure, resonance Raman spectroscopy can be used to obtain the (*n,m*) geometric structure of isolated SWNTs[39,40].

In order to estimate the dopant concentration within SWNTs and MWNTs, analytical techniques associated with HRTEM can be used. In this context, EELS becomes a useful and powerful tool to determine the stoichiometry of elements in individual nanotubes, as well as the nature of the chemical bond. Similarly, XPS can be used to determine stoichiometries of elements and their corresponding binding energies. These techniques are generally only accurate and sensitive to elements at concentrations above 1 at%. Therefore, Raman spectroscopy, which is sensitive to the incorporation of foreign elements, may provide an efficient route to determine dopant concentrations lower than 0.1 at% in SWNTs and MWNTs. The technique may require more development before a quantitative evaluation of the dopant concentration can be determined accurately.

Structure of high temperature synthesized B-doped MWNTs

As mentioned above, B-doped MWNTs produced using the arc method are extremely long (<100 μm), contain more than 20-30 layers, and usually exhibit ill-formed caps (Fig. 2b),

sometimes with a polygonized tubular structure[41]. These caps may also contain higher B concentrations (as revealed by EELS analyses)[42]. This suggests that B acts as a catalyst in the formation of long tubules. Careful EELS studies (using first and second derivative spectra) have shown that minute B traces (<1%) are present within the body of tubules[43]. Although it has been difficult to determine the correct binding energy for B using either EELS or XPS, it is likely that substitutional B (three coordinated) is incorporated in the hexagonal C lattice. ED studies have shown that these long B-doped CNTs exhibit a preferred zigzag or near zigzag chirality (e.g. zigzag ± 3°)[44,45]. Chiralities corresponding to the armchair configuration are rarely observed and other helical arrangements never dominate. It is noteworthy that standard arc-produced MWNTs usually exhibit a change of chirality every four to five graphitic shells, thus leading to turbostratic arrangements[46].

Blase *et al.*[44] have performed static and dynamic *ab initio* calculations and demonstrated that B indeed acts as a surfactant during the growth of long tubes and inhibits tube closure during formation (Fig. 4). This growth model only applies to zigzag tubules (Fig. 4), implying that this nonchiral geometry should be favored in B-doped nanotubes, which also exhibit a high aspect ratio. Hernández *et al.*[47] found similar results for B using tight binding molecular dynamics calculations. Bulk XRD studies on B-doped MWNTs reveal the presence of highly ordered three-dimensional graphite crystals, caused by high intensity (101), (102), (103), and (112) reflections attributed to *ABA*... stacking (Fig. 5). This has never been observed in conventional pure carbon MWNTs or nanoparticles. In addition, B_4C is found as a byproduct. From the (001) reflections (caused by the presence of layers), two different average interlayer spacings arise. These spacings may correspond to standard CNTs/nanoparticles (~3.4 Å) and *AB*-stacked graphite (~3.35 Å), the latter possibly arising from: (i) concentric B-doped zigzag tubes exhibiting *ABA*... stacking; (ii) flattened tube domains (also confirmed by the interlayer spacing irregularities), and (iii) polyhedral particles[41].

Structure and morphology of N-doped MWNTs

The structure of N-doped MWNTs (produced via CVD) has been extensively studied using HRTEM. In general, these tubular structures reveal that: (a) hollow nanofibers possess unusual stacked-cone or compartmentalized morphologies (bamboo-type) (Figs. 6a-b); and (b) the degree of tubular

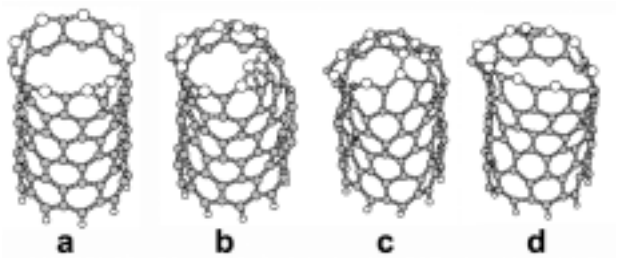

Fig. 4 Snapshots of ab initio molecular dynamics (MD) calculations revealing the formation of B-doped SWNTs with zigzag chirality (9,0). B acts as a surfactant and inhibits tube closure, thus enhancing the length of the tubules. In (a), the ground state geometry at T = 0 K is represented. In (b), (c), and (d) three different snapshots of the nanotube at 2500 K are given. Snapshot (d) represents the final configuration reached by the system at the end of the MD run. Note that the tube shown in (b) contains a pentagon formed by three B atoms and two C atoms. This pentagon leads to partial tube closure and for pure C, the tube would close almost immediately, but the presence of B prevents this and the B-B bond breaks and rearranges along the opposite edge of the tube (d). This demonstrates that B atoms prevents closure of the tubes[44]. (Reprinted with permission from[44]. © 1999 American Physical Society.)

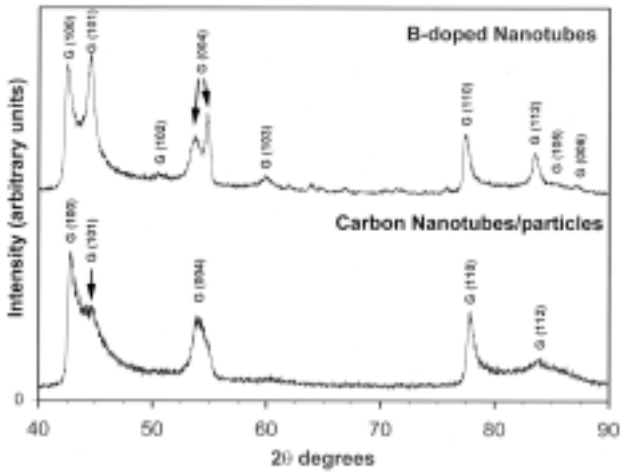

Fig. 5 XRD patterns from the inner core deposits obtained from BN/graphite arc discharge experiments compared with pure MWNTs and nanoparticles. The pattern from 40-90 2θ degrees clearly shows the high degree of crystallinity of the B-doped sample [note the (101), (103), and (112) reflections that denote three-dimensional order and ABAB stacking of the layers]. Also note that the (001) reflection exhibits two peaks corresponding to 3.35 Å and 3.42 Å, thus confirming the presence of two different 'graphitic' structures (graphite-like ABAB... possibly from faceted areas of polygonized nanotubes and turbostratic graphite arising from concentric graphene cylinders, MWNTs).

perfection decreases as a result of N incorporation (Fig. 6c-e). EEL spectra of CN_x nanofibers indicate the presence of ionization edges at ~284.5 eV and 400 eV, corresponding to the C and N K-shells. In some samples, splitting in the π*-type peak of the N K-edge exhibits two features at ~398.7 eV and 400.7 eV. This suggests two bonding types between N and C within the hexagonal network. From EEL spectra, it has been estimated that the N content within the tubes is ~≤10%, commensurate with C_9N_x ($x \leq 1$) stoichiometries.

XPS analyses on N-doped MWNTs[27] confirm the N1s signal splitting at 398.7 eV and 400.9 eV. The latter binding

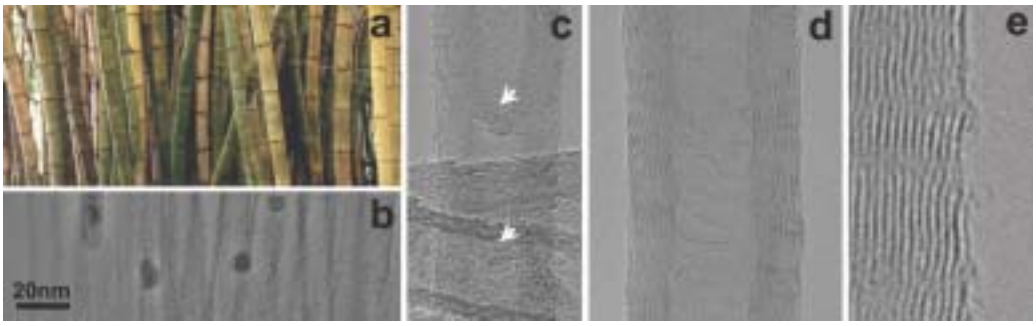

Fig. 6 Images of N-doped MWNTs produced by pyrolysis of melamine in the presence of ferrocene at 900-1050°C. (a) Bundle of bamboo trees resembling the structure of N-doped MWNTs. (b) TEM image of densely packed aligned hollow CN_x nanotubes. Their morphology consists of compartmentalized 'bamboo-like' structures. (c) HRTEM image of an individual CN_x nanotube exhibiting compartments (indicated by arrows), the tube contains ~2 wt% N. (d) HRTEM image of a CN_x nanotube with different morphology from the previous one, where the tubes contain gaseous N_2 in the hollow core; note the rugosity of the surface. (e) Enlargement of (d) exhibiting slight corrugation of the tube surface, the N content is 0.5-1 wt%.

energies correspond to highly coordinated N atoms replacing C atoms within the graphene sheets (~401-403 eV), and to pyridinic N (~399 eV). It is important to note that, as the *overall* N content increases within these structures, the number of graphitic walls within the nanofibers decreases and the proportion of pyridine-like N increases (remaining almost constant with the number of three-coordinated N atoms)[48]. Therefore, the pyridine-like N sites of 'cavities' or 'edges' within the predominantly graphitic framework are responsible for the roughness and the interlinked morphologies observed in these doped nanostructures. This conclusion is consistent with previous theoretical calculations, which indicate that low N concentrations (e.g. 15%) remain in-plane within the hexagonal C framework and form nanostructures with 'smooth' surfaces[49]. Recent theoretical tight binding molecular dynamics calculations have revealed that N incorporation within CNTs should occur for nanotube diameters larger than 8 nm. These calculations are in agreement with experiment[50]. More recently, theoretical calculations using density functional theory have demonstrated that (10,0) zigzag tubes are able to allocate N atoms (far apart and among C atoms) in a homogeneous way, whereas N atoms in (5,5) armchair tubes tend to attach together along the equatorial axis, which is responsible for promoting fracture and instabilities within the tubes[51]. In addition, the authors studied the density of states (DOS) of N-doped nanotubes and demonstrated that substitutional N atoms inject electrons into the conduction band, whereas pyridine-type molecules induce localized states in the valence band[51]. These theoretical studies are now motivating more calculations on the dynamics and electronic structure of doped SWNT systems.

Raman spectroscopy of doped systems

Raman spectroscopy provides a sensitive tool for characterizing CNTs in general and doped nanotubes in particular[40]. For SWNTs, the Raman effect becomes an especially powerful characterization tool, as shown in Fig. 7 for B-doped SWNTs prepared by laser ablation. HRTEM and EELS techniques are not sensitive enough to detect B in SWNTs, and can only give an upper limit of 0.05-0.1 at% to the B concentration[24]. The Raman spectra, taken for B concentrations up to 3 at% in the target, clearly show the presence of SWNTs in the sample because of the observed RBM feature. The results further show, for the samples with 4.5 at% and 10 at% B, there is no evidence of SWNTs within the sample, suggesting that at these higher B concentrations in the target, the B enters the catalytic particles (as shown by EELS measurements) and suppresses nanotube synthesis[24].

A general effect of doping MWNTs, SWNTs, and nanotubes of large and small diameter is observed in the Raman spectra, namely an increase in intensity of the disorder-induced D-band[45,51,52]. The D-band is related to phonon modes that are not Raman active, but appear in the spectra when the crystalline translation symmetry is broken. Upon B doping, the D-band intensity increases for higher doping levels[52]. For example, Figs. 7a and 7b show resonant Raman spectra of SWNT bundles obtained using 1.16 eV (1064 nm) and 2.41 eV (514.5 nm) laser excitation energies. The B levels indicated on Fig. 7 refer to the concentration of B in the target (consisting of a C and B paste) used in the laser ablation synthesis process. The features in the vicinity of (a) 1275 cm^{-1} and (b) 1340 cm^{-1} are associated with the disorder-induced feature (D-band) that appears in each spectrum. The D-band intensity is small in the Raman spectra

of pristine SWNTs and grows in intensity when the graphitic symmetry of sp^2-bonded C atoms is broken by the presence of B atoms along with the attendant disorder introduced by these defects. The D-band frequency is also observed to change with doping concentration. This effect is clearer for the G' band, that is the second-order Raman feature composed by two D-band phonons.

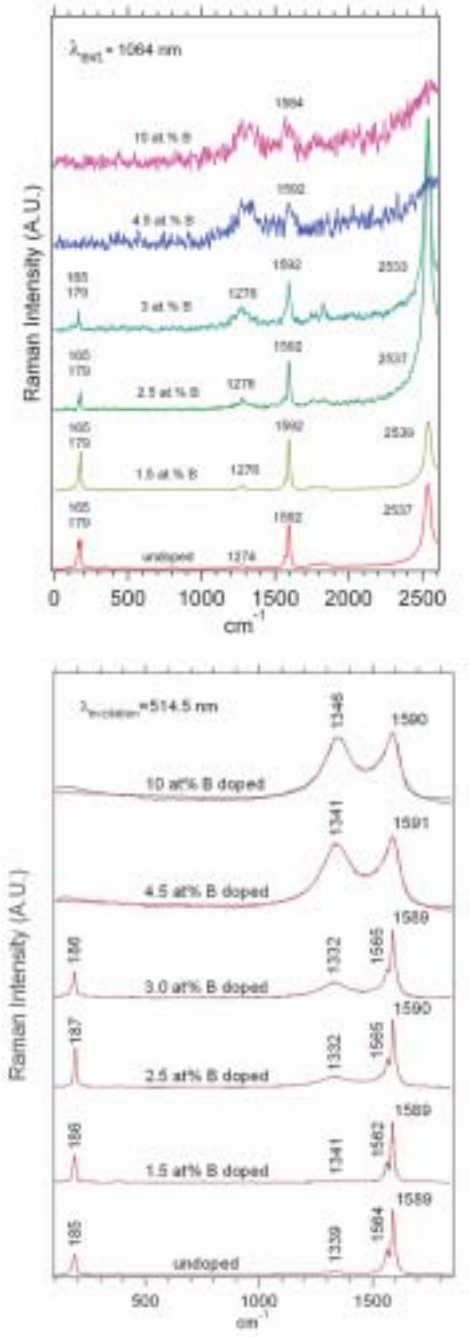

Fig. 7 (a) First- and second-order room temperature Raman spectra of products generated from targets with the indicated B concentrations and excited using the 1064 nm excitation energy. (b) First-order room temperature Raman spectra of products generated from targets with the indicated B concentrations and excited using the 514 nm excitation energy. Note that above 4.5 at% B, SWNTs are notably absent due to the disappearance of the RBM characteristic feature of SWNTs[74] at wave numbers ~186 cm^{-1}. (Reprinted with permission from[24]. © 2004 Royal Society of Chemistry.)

When comparing the D-band in Figs. 7a and 7b, it is clear that this feature exhibits dispersive behavior, i.e. its frequency ω increases with increasing laser excitation energy, E_{laser} ($d\omega/dE_{laser}$ = 53 cm^{-1}/eV). This dispersive behavior is an interesting effect observed in sp^2 carbon materials and is explained by a double resonance process in nanotubes, where the electron/hole that is resonantly excited by the incoming photon can be further resonantly scattered by a specific phonon[53,54]. As discussed above, the phonons involved in this double resonance process are not Raman active and can only be observed in the presence of defects (e.g. doping atoms). The specific morphology of the substitutional doping will probably induce changes in this double resonance process and it is possible that Raman spectroscopy can be used to probe this morphology.

The Raman spectra in Fig. 7a further indicate that, within a given E_{laser}, the frequencies for the RBM at 165 cm^{-1} and 179 cm^{-1} (for which all C atoms are vibrating in phase in the radial direction), the D-band discussed above, and the G-band at 1592 cm^{-1} (for which the nearest neighbor atoms are moving in a tangential direction in a typical optical mode displacement pattern) depend smoothly on B concentration. These features are all excited in a resonance Raman process, whereby the laser excitation energy is very close to a van Hove singularity for the electrons in the strongly quantum-confined, one-dimensional electronic states characteristic of SWNTs. The smooth dependence of the phonon frequencies on the B concentration indicates that the same CNTs are still resonant with E_{laser}, i.e. their singularities in the electronic DOS (at E_{ii}) are not strongly affected by B addition. Whereas Fig. 7a reveals the constancy of the singularity E^S_{22} for semiconducting SWNTs, other spectra taken at 1.96 eV and 2.41 eV show similar phenomena occurring, respectively, at E^M_{11} for metallic SWNTs and E^S_{33} for semiconducting SWNTs.

However, a more careful examination of the spectra in Fig. 7 shows that the intensities of the various phonon modes vary nonlinearly with the concentration of B in the target. When comparing the intensity of different phonon modes in resonance Raman spectroscopy, it is important to consider that resonance can occur for the incident photon (E_{laser}) and for the scattered photon energy (E_{laser} - E_{phonon}). The latter resonance condition varies for different phonons. For

example, the intensity of the RBM in Fig. 7a is largest at 2.5 at% B, indicative of a shift in the resonance condition with B concentration, showing that the presence of B in the SWNT lattice shifts E_{ii} by a few tens of meV, thereby bringing E_{ii} closer (or further) from resonance with the incident (or scattered) photon. Since the resonance condition is best satisfied in Fig. 7a for the G'-band, it is concluded that the resonance is achieved for a laser excitation energy of E_{laser} = 1.16 eV with the scattered photon. In contrast, the dominant resonance has been achieved for the RBM band in Raman measurements at 1.96 eV and 2.41 eV, implying that resonance in these cases is with the incident photon. Raman measurements on individual SWNTs are necessary to yield quantitative information about the diameter and chirality dependence of these phenomena.

Fig. 8 shows that $\omega_{G'}$ down-shifts in frequency with B doping, consistent with the increase in the in-plane lattice constant and a weakening of the B-C in-plane bond strength relative to the corresponding C-C bond, also observed in B-doped graphite[4]. Furthermore, the addition of B introduces holes into the lattice that tend to up-shift the $\omega_{G'}$ frequency,

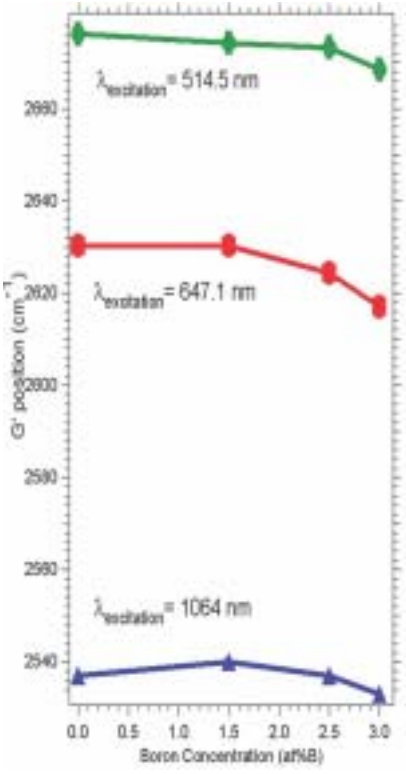

Fig. 8 Softening of $\omega_{G'}$ as a function of B concentration in the target. The down-shift in $\omega_{G'}$ for metallic SWNTs is approximately twice the down-shift exhibited by semiconducting SWNTs[74]. (Reprinted with permission from[24]. © 2004 Royal Society of Chemistry.)

but this effect is smaller than the down-shift produced by the in-plane lattice constant increase with B doping. One remarkable effect, however, is the relatively larger down-shift observed in $\omega_{G'}$ for metallic SWNTs compared with semiconducting SWNTs because of the occupation of states at the Fermi level in metallic SWNTs. Thus the effect of hole addition through B doping moves the Fermi level down slightly from approximately mid-gap, in contrast to semiconducting SWNTs for which the Fermi level drops all the way down to the highest lying van Hove singularity in the valence band. The overall dependence of the D-band frequency ω_D on B doping is consistent, within experimental error, with the general trends of the G'-band in Fig. 8, where a down-shift in ω_D from 1340±2 cm^{-1} for 0 at% and 1.5 at% B traces to 1332±2 cm^{-1} for 2.5 at% and 3.0 at% B traces observed in Fig. 7b at 514.5 nm laser excitation. Essentially no change in ω_D with B doping is observed at 1064 nm laser excitation, also consistent with observations for $\omega_{G'}$ in Fig. 8. To observe effects in the Raman spectra expected for the *c*-axis contraction with B doping, appropriate measurements on MWNTs would have to be carried out.

It is noteworthy that it is possible to relate low B or N content within MWNTs if we compare the intensities of the Raman allowed and disorder-induced modes, so that a low concentration of dopants (e.g. <0.1%) can be detected[52]. Maultzsch *et al.*[52] have demonstrated that it is possible to correlate the concentration of B dopant in MWNTs with D/G' and G/G' intensity ratios, although independent calibration for the proportionality constants and a better understanding of the fundamental issues related to these phenomena are still needed. For SWNTs, it may be possible to relate G-band peaks and RBM intensities so that large differences in the spectra can be related to tiny concentrations of dopants. We believe that Raman spectroscopy may be an ideal way of estimating low dopant concentrations, maybe even specific substitutional structure at the isolated SWNT level, but further theoretical and experimental work is urgently needed.

Theory of transport on doped CNTs

SWNTs exhibit remarkable quantum transport properties[55,56]. For example, the conductance of a one-dimensional conductor is known to have a particularly simple form, according to Landauer's formula, namely the product of the number of conducting channels (two at the Fermi level in the case of SWNTs) and the quantum conductance[57], $G_0 = 2e^2/h$.

First-principle studies of the electronic structure[58] and quantum transport in short CNT devices containing a single doping atom (B or N) using the Landauer[59] and Keldysh[60] formalisms reveal the presence of localized states around the substituting impurity. These quasibound states are responsible for the enhancement of backscattering for energies below (B doping) or above (N doping) the charge neutrality point. The quasibound states in metallic nanotubes with B and N impurities have a similar physical origin as that of acceptor or donor levels in typical semiconductors or semiconducting nanotubes[61]. The quasibound levels associated with B are close to the first lower subband (and derived mainly from it), analogous to the acceptor level in semiconductors, except that they are in resonance with the continuum of conducting states. Likewise, the quasibound states associated with the N impurity behave similarly to the donor states in semiconductors[59]. Consequently, a substitutional B (N) impurity produces quasibound states made of π orbitals perpendicular to the tube surface below (above) the Fermi energy, leading to a reduction in conductance at the corresponding quasibound state energies.

Recently, generic transport properties such as conduction mechanisms, mean-free-paths, and conductance scalings have been derived for various concentrations of B and N dopants randomly distributed within the honeycomb network of SWNTs[62] using a theoretical technique based on the tight-binding formalism correlated with *ab initio* calculations. These theoretical calculations, which take into account both the charge transfer and elastic scattering associated with dopants, reveal that electronic transport depends strongly upon the doping rate. A low density of dopants yields diffusive regimes, with a mean-free-path decreasing linearly with dopant concentration and increasing linearly with nanotube diameter. The calculated mean-free-paths for B-doped nanotubes with diameters in the range 17-27 nm, and 1.0% doping are in the order of 175-275 nm, which is in agreement with experimental estimations[63]. These calculations show that a small amount of dopant can drastically modify the electronic transport properties of the tube, which is a key effect for future nanoelectronics.

In addition, conductance scaling in the quantum coherent regime has been analyzed for B- and N-doping. In both cases, as the typical length of the device increases from the nanometric (~10 nm) to the mesoscopic scale (~1 μm), quantum interference effects beyond the diffusive regime are correspondingly enhanced. A strong asymmetric damping of the electronic conductance is thus observed. The generic conductance of a B- (N-) doped CNT device exhibits a positive (negative) derivative with respect to the energy at the Fermi level. This difference in the conductance between B- and N-doped CNTs suggests that the thermopower measurements originate from a diffusion mechanism only[64].

Although some experimental transport measurements have been reported recently in B-doped nanotubes, typically with a few percent of dopants, and metallic nanotubes with mesoscopic length scales[65], little is known about intrinsic transport length scales in such hetero-atomic nanostructures. Experimental studies on chemically doped CNTs would be useful to confirm these theoretical predictions. For thermal transport on doped nanotubes, one would expect a reduction because of increased phonon scattering. To the best of our knowledge, there are neither experiments nor calculations on the thermal properties of B- and N-doped nanotubes.

Measurements of electronic transport

To the best of our knowledge, the electronic properties of individual B- or N-doped SWNTs have not been reported. However, microwave conductivity measurements on bulk B-doped MWNTs reveal that these structures are intrinsically metallic[66], which is different from standard pure CNTs that show thermally-activated transport. Carroll *et al.*[67] detected characteristic peaks in the DOS using STS on B-doped MWNTs (Fig. 9a). The peaks that appear in the valence band are caused by the introduction of B (which acts as an acceptor) in the C lattice (Fig. 9a). The authors suggest that BC_3 islands, distributed within the tubules, significantly alter the local DOS (LDOS) from a semimetal to an intrinsic metal. The results have been confirmed by *ab initio* calculations, indicating that the changes in the electronic structure arise mainly from the presence of dopant-rich islands and not isolated substitutional B atoms[67].

Electronic transport measurements on individual B-doped MWNTs reveal metallic[63] behavior above 30 K, which results from an enhancement in conduction channels without strong backscattering. In addition, the *dI/dV* versus *V* curves of MWNTs exhibit a small peak close to the Fermi level (Fig. 9c) which is associated with the presence of acceptor states caused by BC_3 islands. At lower temperatures, the resistance starts to increase. The results suggest that B-doping induces *p*-type behavior within MWNTs[63].

Electron spin resonance (ESR) studies have confirmed the intrinsic metallic behavior of bulk B-doped MWNTs[68]. In particular, a *g*-value of 2.002 at room temperature has been observed for B-doped nanotubes, whereas the typical value for pure CNTs is 2.0189. Furthermore, superconducting quantum interference device (SQUID) measurements have demonstrated that the bulk material is paramagnetic (standard CNTs are strongly diamagnetic), exhibiting a weak temperature dependence of the magnetization commensurate with a metallic response.

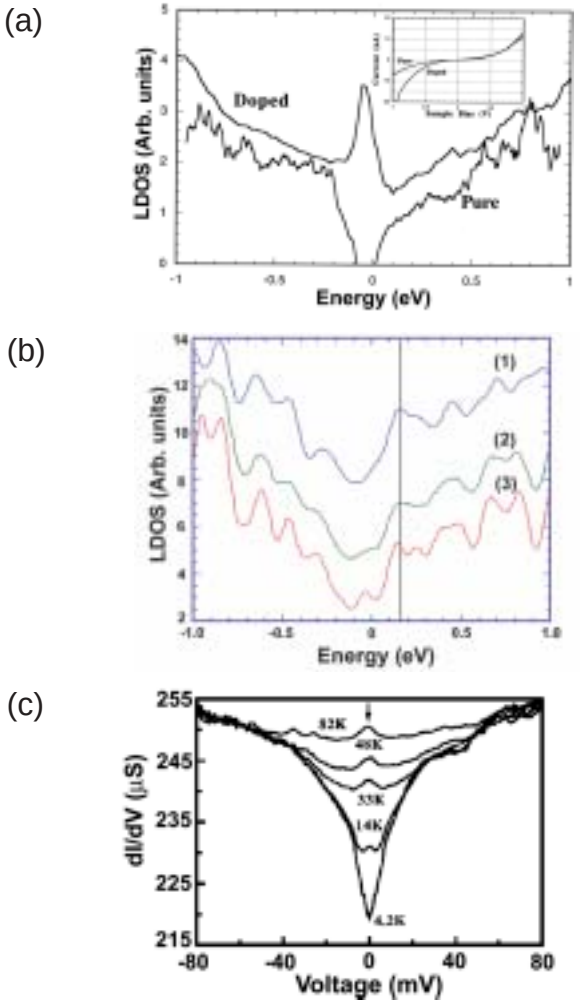

Fig. 9 (a) LDOS of a B-doped MWNT showing a clear peak in the valence band caused by the presence of B atoms in the tube[67]. A possible explanation is based upon the existence of BC_3 islands within the hexagonal carbon network. (Courtesy of P. M. Ajayan and D. L. Carroll. Reprinted with permission from67. © 1998 American Physical Society.) (b) Tunneling spectra acquired on a straight, clean section of a CN_x nanotube. Spectra 1-3 were taken at different locations along the surface but close to a 'hole' (CN bond)[69]. Note the peak at 0.18 eV (conduction band) in all spectra (see vertical line). (Reprinted with permission from[69]. © 2001 American Chemical Society.) (c) dI/dV versus V curves of an individual MWNT doped with B exhibiting a small peak close to E_f, which is associated with the presence of an acceptor (B); peak due to B indicated by an arrow[63]. (Reprinted with permission from[63]. © 2001 American Physical Society.)

STM and STS studies have revealed that N-doped MWNTs are metallic and exhibit a characteristic peak in the conduction band DOS (Fig. 9b). For pure CNTs, the valence and conduction band features appear to be symmetric about the Fermi level, whereas N-doped MWNTs have an additional electronic feature at ~0.18 eV (Fig. 9b). This result is in contrast to the B-doped case[69]. It is noteworthy that the electron donor feature observed in N-doped material is always seen along doped nanotubes. Therefore, both two- and three-coordinated N (substitutional and pyridinic, respectively), randomly distributed within armchair and zigzag CNTs, should lead to these prominent donor peaks close above the Fermi energy (at ~0.18 eV). Careful *ab initio* calculations are now under way to explain the exact type of C-N bond within the tubes. More recently, it has been shown that CN_x nanotubes are indeed metallic[70] (Fig. 10a) and could behave as efficient electron field emitters (Fig. 10b).

Thermoelectric power measurements (TEP) are sensitive to the carrier sign of any material. Since TEP is a zero current transport coefficient, it is able to probe the intrinsic conduction properties of individual nanotubes[71] because it is less influenced by randomly entangled morphologies and

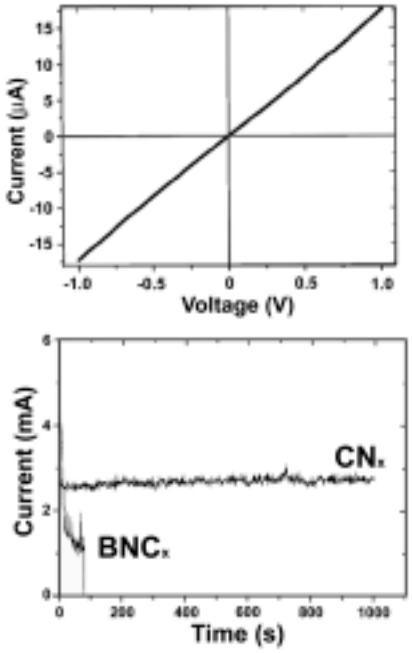

Fig. 10 (a) I-V characteristics of a rope of N-doped MWNTs. The rope displays stable field emission and a marked low-resistance metallic behavior (linear I–V curve, R ~70 K). (b) Plot of the field-emission stability of N-doped MWNT CN_x compared to BNC_x ($x < 0.1$). CN_x nanotube film emission is stable at low and high current densities. Note that BNC_x nanotubes do not show stable electron emission[70]. (Reprinted with permission from[70]. © 2003 Springer-Verlag.)

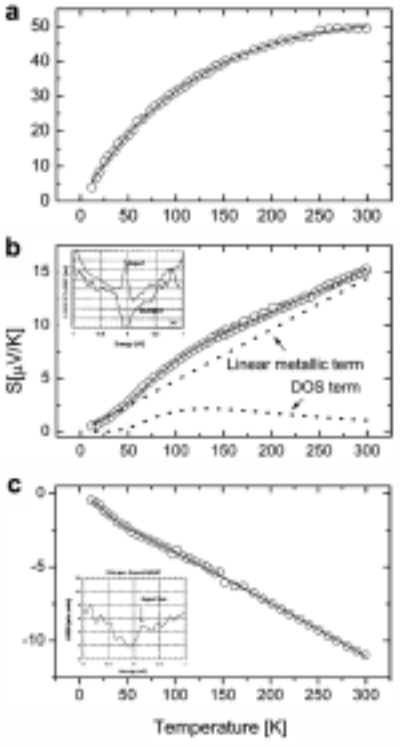

Fig. 11 Thermopower measurements performed on doped and undoped MWNTs. (a) TEP of a pure MWNT mat and a fit by a heterogeneous model (solid line). (b) TEP of a B-doped MWNT mat and a fit (solid line) indicating positive (hole) carriers. The dotted lines show the effect of the linear metallic term (straight line) and the DOS term. The DOS peak results in a broader peak in S. (c) TEP of N-doped MWNT mat indicating negative (electron) carriers and fit (solid line)[64]. (Reprinted with permission from[64]. © American Chemical Society.)

imperfections in the measured mats compared with standard conductivity measurements. Recently, TEP measurements of B- and N-doped MWNT mats have been carried out and compared with pure carbon MWNTs (Fig. 11)[64]. These studies demonstrate that the TEP of B-doped MWNTs is positive (Fig. 11b), thus indicating hole-like carriers. In contrast, N-doped tubes exhibit negative TEP over the same temperature range (Fig. 11c), suggesting electron-like conduction[64]. These results could be correlated to the DOS for B- and N-doped MWNTs. It is important to note that as-produced, pure carbon MWNTs exhibit positive TEP (Fig. 11a), which has been attributed to the presence of O dopants. If the sample is left in vacuum for 94 hours, the TEP signal decreases considerably[64,71]. In this context, it is important to note that TEP studies of SWNTs have been able to indicate alkali metal intercalation[72] and O contamination (or doping)[73]. Recently, McGuire and coworkers[74] have demonstrated that B-doped SWNTs (produced using laser ablation) display positive TEP values (Fig. 12), thus implying the presence of holes (as for B-doped MWNTs). These clear

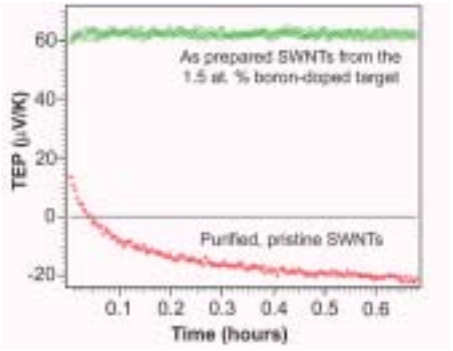

Fig. 12 Comparison of the TEP data for purified, pristine SWNTs and SWNTs produced from a nominal 1.5 at% B-doped target. In both data sets[74] the sample was held at 500 K and 10^{-6} torr. (Reprinted with permission from[24]. © 2004 Royal Society of Chemistry.)

changes in the TEP occur for very low B concentrations (e.g. 0.05-0.1 at% B), too low to be detected by EELS or XPS. Therefore, TEP measurements are extremely sensitive to low doping levels of B (or N) within SWNTs and MWNTs. Therefore, further studies are necessary. Returning to Fig. 12, it is important to note that at 500 K and 10^{-5} torr, the TEP of air-exposed pristine SWNT bundles changes sign (from positive to negative), whereas B-doped bundles resist this change, implying that B-doping lends them permanently *p*-type characteristics.

At present, thermal conductivity measurements on B- and N-doped CNTs with different dopant concentrations should be performed. It is clear that, depending on the doping level, the electronic and thermal properties will vary drastically, since the conductivity of undoped nanotubes is dominated by the lattice. Therefore, doping may provide a handle on probing electronic contributions to thermal conductivity.

Applications & emerging technologies

Field emission Electrons can be easily emitted from CNT tips when a potential is applied between the CNT surface and an anode. In particular, Charlier *et al.*[42] have reported that B-doped MWNTs could exhibit enhanced field emission (turn on voltages of ~1.4 V/μm) when compared to pristine carbon MWNTs (turn on voltages of ~3 V/μm) (Fig. 13a). This phenomenon arises from the preferential presence of B atoms at the nanotube tips, which results in an increased DOS close to the Fermi level. In addition, tight binding and *ab initio* calculations demonstrate that the work function of B-doped CNTs is much lower (1.7 eV) than that observed in pure carbon MWNTs (Fig. 13b and 13c). Similarly, Golberg *et al.*[70] have demonstrated that N-doped MWNTs are able to emit electrons at relatively low turn-on voltages (2 V/μm) and

high current densities (0.2-0.4 A/cm^2). More recently[75], individual N-doped MWNTs have shown excellent field emission properties at 800 K; experimental work functions of 5 eV and emission currents of ~100 nA obtained at ±10 V. Thus, both B- and N-doped CNTs may have great potential as building blocks for stable and intense field-emission sources. Further work should now be carried out on the field-emission properties of B- and N-doped SWNTs.

Li$^+$ batteries Lithium is a metal, which easily donates electrons from Li$^+$, and has proved to be extremely important for the fabrication of lightweight and energy-efficient batteries. When using graphite-like materials in Li$^+$ batteries, the ions are intercalated between the graphite layers, so that Li$^+$ migrates from a graphitic anode to the cathode (usually $LiCoO_2$, $LiNiO_2$, and $LiMn_2O_4$). The theoretical Li storage capacity in graphite is 372 mAh/g (LiC_6), and the charge and discharge phenomenon in these batteries is based upon the Li$^+$ intercalation and de-intercalation[76]. Nowadays, various electronic companies commercialize such batteries in portable computers, mobile telephones, digital cameras, etc. Endo and coworkers[76] have proved that B-doped vapor grown carbon fibers (VGCFs) and carbon nanofibers are far superior to any other carbon source present in the graphitic anode. This may be because the population of Li$^+$ has a stronger affinity to B-doped sites, resulting in a higher energy storage for the battery arising from the increase in the cycle characteristics[76,77]. N-doped CNTs and nanofibers have also shown efficient reversible Li storage (480 mAh/g); much higher than commercial carbon materials used for Li$^+$ batteries (330 mAh/g)[78].

Sensors It has been demonstrated by various groups[79-81] that pure carbon SWNTs and MWNTs can be used to detect toxic gases and other species, because small concentrations are capable of producing large changes in the nanotube conductance, shifting the Fermi level to the valence band, and generating hole-enhanced conductance[79]. However, N-doped MWNTs have proved more efficient in this context. In particular, CN_x MWNTs display a fast response on the order of milliseconds when exposed to toxic gases and organic solvents (Fig. 14)[82], and reach saturation within 2-3 seconds. In all cases, an increase in the electrical resistance is caused by the presence of molecules strongly bound to the pyridine-

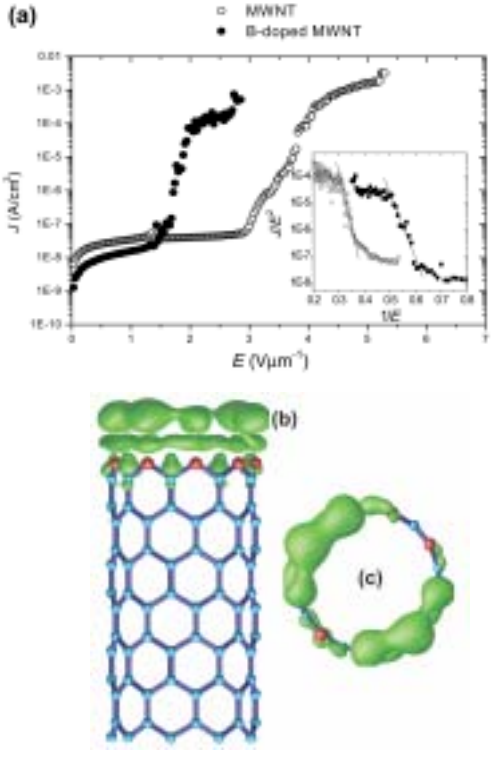

Fig. 13 (a) J-E emission characteristics, measured in parallel plate configuration, of B-doped MWNT films and comparable films of pure carbon arc-produced MWNTs. The plate area was 0.25 cm^2. Inset shows the Fowler-Nordheim plots for each curve. The calculated field enhancement factor β was found to be ~1000. Side (b) and top (c) views of localized states at the edges of a B-saturated zigzag (9,0) CNT computed using ab initio calculations. The work function of this tube is 1.7 eV lower than that of the same nanotube made exclusively of C atoms. (Reprinted with permission from[42]. © American Chemical Society.)

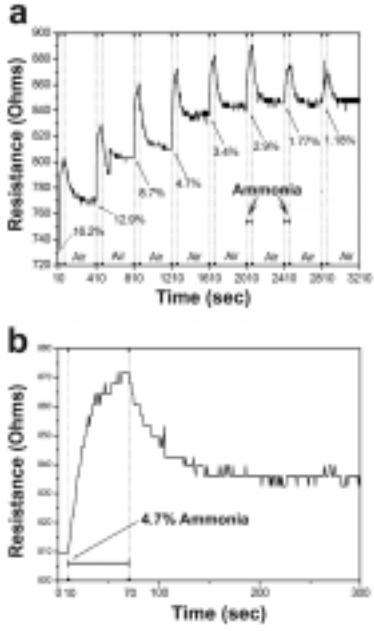

Fig. 14 Plots of resistance versus time for NH_3 on N-doped MWNT sensors. (a) It is clear that the sensor is sensitive to ~1% NH_3. Chemisorption is clearly observed, which can be attributed to the strong interactions between the pyridinic sites of the tube surface with the NH_3 molecule; (b) graph indicating the response time for NH_3 gas (4.7%)[82]. The results demonstrate that N-doped MWNTs could be used in the fabrication of novel and fast responsive gas sensors. (Reprinted with permission from[82]. © 2004 Elsevier Ltd.)

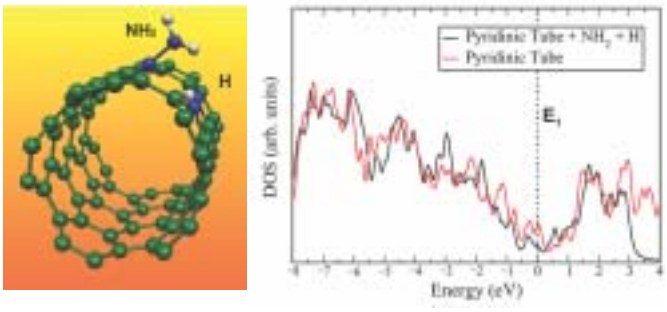

Fig. 15 Molecular models for (5,5) CNTs doped with pyridinic sites on their surface and molecules adsorbed in the vicinity of this region for NH_3. Next to the plot, the total DOS of the structure is presented. Note that the electronic states decrease at E_f, indicating reduced electronic conduction in the functionalized tubes. We observed that the most stable configuration is an amino (NH_2) group bonded to an N atom, with the other H atoms atoms connected to other N atoms present in the pyridinic region[82]. (Reprinted with permission from[82]. © 2004 Elsevier Ltd.)

like sites present within the CN_x nanotubes (Fig. 14). For ethanol, acetone, and NH_3, a permanent change to higher values has been observed in the resistance, which has been confirmed using first-principles calculations[82]. In particular, a clear decrease in the DOS at the Fermi level is observed, indicative of lower conduction and chemisorption (Fig. 15). Therefore, CN_x nanotubes could potentially be more efficient in quickly detecting gaseous hazardous species because of the presence of reactive sites (mainly pyridine-type) on their surface. In this context, B-doped CNTs should be tested for this application. Theoretical *ab initio* calculations have demonstrated that CO and H_2O molecules do not react with the surface of pure carbon SWNTs[83]. If the surface of the tube is doped with a donor or an acceptor, drastic changes in the electronic properties are observed as a result of the binding of the molecules to the doped locations[82,83]. We envisage that either CN_x nanotubes or B-doped MWNTs could be used to detect low concentrations of ethanol, important in the fabrication of alcohol meters. Therefore, further work is needed in this area and experiments using doped SWNTs should be carried out.

Composites In order to fabricate nanotube composites exhibiting good performance, the formation of stable tube-surface-polymer interfaces is crucial. In this case, the surface of highly crystalline MWNTs tends to be similar to graphite, and chemically 'inert'. Therefore, surface modification treatments are required so that efficient tube-matrix interactions can be established[84]. In this context, the creation of nanotubes containing a few foreign atoms in the hexagonal network such as N or B could circumvent this problem. In some cases, the mechanical properties would not be altered significantly because these 'doped' structures would preserve their outstanding mechanical properties since the level of doping is low (<1-2%)[15]. Preliminary studies on the preparation of epoxy composites using N-doped MWNTs have revealed an increase of 20°C in the glass transition temperature with incorporation of 2.5 wt% CN_x MWNTs using dynamic mechanical thermal analysis (DMTA)[85]. Recently, it has been possible to create active N-rich sites for covalently attaching proteins[86], molecules, and Au clusters[87] to the surfaces of N-doped MWNTs. At present, mechanical measurements on these doped nanosystems should also be carried out and novel conducting polymer composites (*p*- or *n*-type) exhibiting outstanding mechanical and thermal characteristics should be devised.

Summary

We have demonstrated that CNTs doped with B or N should exhibit novel electronic, chemical, and mechanical properties that are not found in their pure carbon counterparts. However, and in order to exploit these novel properties fully, low concentrations of dopants (e.g. <0.5%) should be incorporated within these tubes. In this way, the electronic conductance would be significantly enhanced and the mechanical properties would not be altered. In addition, because of the presence of holes (B-doped tubes) or donors (N-doped tubules), their surface would become more reactive. This reactivity would be extremely useful in the development of field-emission sources, nanoelectronics, sensors, and strong composite materials. It is noteworthy that efficient routes to dope SWNTs should have priority if quantum properties are to be achieved. Unfortunately, not much work in these areas has so far been performed and much more is needed. We foresee that B- and N-doped SWNTs are likely to become more useful than undoped material. Therefore, further experimental and theoretical research should now be concentrated in these areas. MT

Acknowledgments

We are indebted to S. Latil, P. M. Ajayan, X. Blase, D. Golberg, R. Kamalakaran, M. Reyes-Reyes, V. Meunier, F. Villalpando-Páez, A. H. Romero, E. Muñoz-Sandoval, N. Grobert, Ph. Redlich, D. L. Carroll, R. Czerw, A. K. Cheetham, M. Rühle, Y. Bando, K. McGuire, P. L. Gai, R. Rao, G. Keskar, D. Ramírez-González, and L. Noyola-Cherpitel for stimulating discussions and valuable assistance in some of the work reviewed here. MT and HT are grateful to CONACYT-México (grants: W-8001-millennium initiative, 37589-U, 36365-E, UC-MEXUS PS/CN 02-144) and the CIAM initiative (grants CO2-41464 and CO2-42428) for financial support. MSD and GD gratefully acknowledge support from NSF-DMR-01-16042. A. Jorio acknowledges financial support from the Instituto de Nanosciências, CNPq, Brazil. AMR acknowledges support from NSF NIRT 0304019.

REFERENCES

1. Dresselhaus, M. S., *et al., Science of Fullerenes and Carbon Nanotubes*, Academic Press, New York (1996)
2. Terrones, M., *Ann. Rev. Mater. Res.* (2003) **33**, 419
3. Terrones, M., and Terrones, H., *Philos. Trans. R. Soc. London, Ser. A* (2003) **361**, 2789
4. Lowell, C. E., *J. Am. Ceram. Soc.* (1966) **50**, 142
5. Hach, C. T., *et al., Carbon* (1999) **37**, 221
6. Oya, A., *et al., Fuel* (1979) **58**, 495
7. Allen, S., *et al., Nature* (1969) **224**, 684
8. Endo, M., *et al., J. Appl. Phys.* (2001) **90**, 5670
9. Endo, M., *et al., Carbon* (1999) **37**, 561
10. Zanchetta, J. V., and Marchand, A., *Carbon* (1966) **3**, 332
11. Takeya, K., and Yazawa, K., *J. Phys. Soc. Jpn.* (1964) **19**, 138
12. Takeya, K., *et al., Phys. Rev. Lett.* (1965) **15**, 111
13. Belz, T., *et al., Carbon* (1998) **36**, 731
14. Hernández, E., *et al., Phys. Rev. Lett.* (1998) **80**, 4502
15. Hernández, E., *et al., Appl. Phys. A. Mater.* (1999) **68**, 287
16. Gao, R., *et al., Phys. Rev. Lett.* (2000) **85**, 622
17. Gaillard, J., *et al.*, unpublished results
18. Stephan, O., *et al., Science* (1994) **266**, 1683
19. Redlich, Ph., *et al., Chem. Phys. Lett.* (1996) **260**, 465
20. Terrones, M., *et al., Fullerene Sci. Technol.* (1998) **6**, 787
21. Hsu, W. K., and Terrones, M., unpublished results
22. Glerup, M., *et al., Chem. Phys. Lett.* (2004) **387**, 193
23. Zhang, Y., *et al., Chem. Phys. Lett.* (1997) **279**, 264
24. Gai, P. L., *et al., J. Mater. Chem.* (2004) **14**, 669
25. Terrones, M., *et al., Chem. Phys. Lett.* (1996) **259**, 568
26. Terrones, M., *et al., Nature* (1997) **388**, 52
27. Terrones, M., *et al., Adv. Mater.* (1999) **11**, 655
28. Sen, R., *et al., J. Mater. Chem.* (1997) **7**, 2335
29. Dai, H., *et al., Chem. Phys. Lett.* (1996) **260**, 471
30. Cheng, H. M., *et al., Appl. Phys. Lett.* (1998) **72**, 3282
31. Oberlin, A., *et al., J. Cryst. Growth* (1976) **32**, 335
32. Keskar, G., *et al., Chem. Phys. Lett.* (2004), submitted
33. Golberg, D., *et al., Carbon* (2000) **38**, 2017
34. Borowiak-Palen, E., *et al., Chem. Phys. Lett.* (2003) **378**, 516
35. Wang, E. G., *et al., Carbon* (2003) **41**, 1827
36. Teo, K. B. K., *et al., Appl. Phys. Lett.* (2001) **79**, 1534
37. Teo, K. B. K., *et al., Nano Lett.* (2004) **4**, 921
38. Yu, J., *et al., Chem. Phys. Lett.* (2000) **323**, 529
39. Jorio, A., *et al., New J. Phys.* (2003) **5**, 139
40. Dresselhaus, M. S., *et al., Carbon* (2002) **40**, 2043
41. Terrones, M., *et al., Carbon* (2002) **40**, 1665
42. Charlier, J.-C., *et al., Nano Lett.* (2002) **2**, 1191
43. Kohler-Redlich, Ph., and Terrones, M., unpublished results
44. Blase, X., *et al., Phys. Rev. Lett.* (1999) **83**, 5078
45. Hsu, W. K., *et al., J. Mater. Chem.* (2000) **10**, 1425
46. Liu, M., and Cowley, J. M., *Carbon* (1994) **32**, 393
47. Hernández, E., *et al., J. Chem. Phys.* (2000) **113**, 3814
48. Terrones, M., *et al., Appl. Phys. Lett.* (1999) **75**, 3932
49. dos Santos, M. C., and Alvarez, F., *Phys. Rev. B* (1998) **58**, 13918
50. Srivastava, D., *et al., Phys. Rev. B* (2004) **69**, 153414
51. Kang, H. S., and Jeong, S., *Phys. Rev. B* (2004), in press
52. Maultzsch, J., *et al., Appl. Phys. Lett.* (2002) **81**, 2647
53. Thomsen, C., and Reich, S., *Phys. Rev. Lett.* (2000) **85**, 5214
54. Saito, R., *et al., Phys. Rev. Lett.* (2002) **88**, 027401
55. White, C. T., and Todorov, T. N., *Nature* (1998) **393**, 240
56. Frank, S., *et al., Science* (1998) **280**, 1744
57. Chico, L., *et al., Phys. Rev. B* (1996) **54**, 2600
58. Nevidomskyy, A. H., *et al., Phys. Rev. Lett.* (2003) **91**, 105502
59. Choi, H. J., *et al., Phys. Rev. Lett.* (2000) **84**, 2917
60. Kaun, C.-C., *et al., Phys. Rev. B* (2002) **65**, 205416
61. Yi, J.-Y., and Bernholc, J., *Phys. Rev. B* (1993) **47**, 1708
62. Latil, S., *et al., Phys. Rev. Lett.* (2004), in press
63. Liu, K., *et al., Phys. Rev. B* (2001) **63**, 161404
64. Choi, Y.-M., *et al., Nano Lett.* (2003) **3**, 839
65. Krstic, V., *et al.,, Phys. Rev. B* (2003) **67**, 041401
66. Terrones, M., *et al., Appl. Phys. A* (1998) **66**, 307
67. Carroll, D. L., *et al., Phys. Rev. Lett.* (1998) **81**, 2332
68. Hsu, W. K., *et al., Chem. Phys. Lett.* (2000) **323**, 572
69. Czerw, R., *et al., Nano Lett.* (2001) **1**, 457
70. Golberg, D., *Appl. Phys. A* (2003) **76**, 499
71. Sumanasekera, G. U., *et al., Phys. Rev. Lett.* (2000) **85**, 1096
72. Grigorian, L., *et al., Phys. Rev. B* (1998) **58**, R4195
73. Bradley, K., *et al., Phys. Rev. Lett.* (2000) **85**, 4361
74. McGuire, K., *et al.,* unpublished results
75. Doytcheva, M., *et al., Chem. Phys. Lett.* (2004), in press
76. Endo, M., *et al., Carbon* (2001) **39**, 1287
77. Mukhopadhyay, I., *et al., J. Electrochem. Soc.* (2002) **149**, A39
78. Zhang, D. Y., *et al., Appl. Phys. Lett.* (2001) **79**, 3500
79. Kong, J., *et al., Science* (2000) **287**, 622
80. Wong, S. S., *et al., Nature* (1998) **394**, 52
81. Collins, P. G., *Science* (2000) **287**, 1801
82. Villalpando-Páez, F., *et al., Chem. Phys. Lett.* (2004) **386**, 137
83. Peng, S., and Cho, K., *Nano Lett.* (2003) **3**, 513
84. Calvert, P., *Nature*, (1999) **399**, 210
85. Eitan, A., *et al., Proceedings of the 10th US-Japan Conference on Composite Materials* (2002), 634
86. Jiang, K., *et al., J. Mater. Chem.* (2004) **14**, 37
87. Jiang, K., *et al., Nano Lett.* (2003) **3**, 275

FURTHER READING

- Saito, R., *et al., Physical Properties of Carbon Nanotubes*, World Scientific, New York (1998)
- Harris, P. J. F., *Carbon Nanotubes and Related Structures*, Cambridge University Press, Cambridge (1999)
- Dresselhaus, M. S., *et al., Carbon Nanotubes: Synthesis, Structure and Applications*, Springer-Verlag (2000)
- Terrones, M., and Terrones, H., (eds.), Nanotechnology of Carbon and Related Materials. In: *Philos. Trans. R. Soc. London* (2004)